Journal Pre-proofs

Correlating mechanical and rheological filament properties to processability and quality of 3D printed tablets using multiple linear regression

Klemen Kreft, Zoran Lavrič, Urška Gradišar Centa, Mohor Mihelčič, Lidija Slemenik Perše, Rok Dreu

PII: S0378-5173(23)01141-9
DOI: https://doi.org/10.1016/j.ijpharm.2023.123719
Reference: IJP 123719

To appear in: *International Journal of Pharmaceutics*

Received Date: 19 September 2023
Revised Date: 14 December 2023
Accepted Date: 15 December 2023

Please cite this article as: K. Kreft, Z. Lavrič, U. Gradišar Centa, M. Mihelčič, L. Slemenik Perše, R. Dreu, Correlating mechanical and rheological filament properties to processability and quality of 3D printed tablets using multiple linear regression, *International Journal of Pharmaceutics* (2023), doi: https://doi.org/10.1016/j.ijpharm.2023.123719

Correlating mechanical and rheological filament properties to processability and quality of 3D printed tablets using multiple linear regression

Klemen Kreft[a, b], Zoran Lavrič[a], Urška Gradišar Centa[c], Mohor Mihelčič[c], Lidija Slemenik Perše[c], Rok Dreu[a,*]

*Corresponding author.

E-mail address: rok.dreu@ffa.uni-lj.si (R. Dreu)

[a] Faculty of Pharmacy, University of Ljubljana, Aškerčeva cesta 7, 1000 Ljubljana, Slovenia

[b] Lek d.d., Verovškova 57, 1526 Ljubljana, Slovenia

[c] Faculty of Mechanical Engineering, University of Ljubljana, Aškerčeva cesta 6, 1000 Ljubljana, Slovenia

Abstract

Filament formulation for FDM is a challenging and time-consuming process. Several pharmaceutical polymers are not feedable on their own. Due to inadequate filament formulation, 3D printed tablets can also exhibit poor uniformity of tablet attributes. To better understand filament formulation process, 23 filaments were prepared with the polymer mixing approach. To yield processable filaments, brittle and pliable polymers were combined. A 20 % addition of a pliable polymer to a brittle one resulted in filament processability and vice versa. Predictive statistical models for filament processability and uniformity of tablet attributes were established based on the mechanical and rheological properties of filaments. 15 input variables were correlated to 9 responses, which represent filament processability and tablet properties, by using multiple linear regression approach. Filament stiffness, assessed by indentation, and its square term were the only variables that determined the filament's feedability. However, the resulting model is equipment-specific since different feeding mechanism exert different forces on the filaments. Additional models with good predictive power (R^2_{pred} > 0.50) were established for tablet width uniformity, drug release uniformity, tablet disintegration time uniformity and occurrence of disintegration, which are equipment-independent outputs. Therefore, the obtained model outcomes could be used in other research endeavours.

Keywords: Fused deposition modelling, Personalized medicine, Multiple linear regression, Tablet quality attributes, Correlation, 3D printing

1. Introduction

Since the expiration of key patents in additive manufacturing and approval of the first 3D printed medication, 3D printing has experienced considerable activity in the medical field. The technology is attractive to say the least, as it allows complete control over the design of the printed object. Growing awareness of the benefits of widespread use of personalized medicine, supported by the achievements of pharmacogenomics, emerged at virtually the same time, linking both personalized medicine and manufacturing technology into a potential platform for drug manufacturing of the future. Tailored dimensions and dosage strength for each individual patient would greatly improve the quality of life, boost treatment effectiveness, reduce drug adverse effects and increase patient compliance (Siamidi et al., 2020; Trenfield et al., 2018). Various implementations of this rapid 3D prototyping technology have been developed, such as fused deposition modelling (FDM), selective laser sintering, stereolithography, binder jetting, semi-solid extrusion and many more (Jamróz et al., 2018).

FDM is especially enticing due to low cost, wide variety of 3D printer manufacturers and relatively short production times (Jamróz et al., 2018; Lamichhane et al., 2019). Many researchers have proved the viability of FDM for production of 3D printed solid dosage forms (Tan et al., 2018). Furthermore, connecting hot-melt extrusion (HME) with the 3D printing process provides a capable machinery for personalized medicine production in a two-step process. HME is first utilized to turn a polymer-based powder mixture into the filament, a feedstock for 3D printing. The filament is subsequently loaded into the FDM 3D printer via a filament spool. Upon passing the heated nozzle, the polymer changes from a solid glassy to a viscoelastic rubbery state. The polymer's viscosity is reduced, and the significantly softened filament is deposited onto the print bed in several layers. The material then cools down, as the individual layers merge together into a solid structure. 3D printer deposits the filament based on the computer-aided design (CAD) (Jamróz et al., 2018).

Most pharmaceutical thermoplastic polymers show a lot of promise for hot-melt extrusion and filament formation due to high thermal stability, good solubilization capacity, adequate viscosity at printing temperature and biocompatibility. Polyvinyl alcohol (PVA), polyvinyl pyrrolidone (PVP), polyvinyl alcohol-polyethylene glycol graft copolymer (Kollicoat®IR), cellulose derivatives (HPC, HPMC, EC, HPMCAS), polymethacrylate-based copolymers etc. have all been investigated as potential API carriers (Azad et al., 2020; Melocchi et al., 2016; Palekar et al., 2019; Pietrzak et al., 2015; Zhang et al., 2017). However not many are printable on their own, mostly due to excessive brittleness or pliability. In the pharmaceutical industry, it is desirable that HME extrudates exhibit brittle behavior to allow for postprocessing, such as comminution, pellet or tablet manufacturing. On the other hand, filaments for 3D printing require a compromise between pliability, hardness and stiffness to pass the nozzle without excessive damage (Aho et al., 2019; Nasereddin et al., 2018; Palekar et al., 2019).

The filament feeder aggressively handles the filament during the feeding process. The drive and pinch wheels squeeze the feedstock material and send it into the printing head liquefier for material deposition at high shear rates. During the feeding process, the filament can become damaged with small indentations (Go et al., 2017). This can result in filament breakage within the feeder. In addition, soft and pliable filaments can buckle before or within the printhead. The filament gets stuck when entering the liquefier due to the lack of column strength along the material (Ilyés et al., 2019; Solanki et al., 2018). Filament buckling can be otherwise somehow managed by establishing a critical ratio between the filament's elastic modulus and apparent viscosity (Venkataraman et al., 2000). Filament residue within the printhead is also problematic from the cleaning standpoint, as the mechanism needs to be completely disassembled to remove the debris and residuals (Nasereddin et al., 2018). As a result, good mechanical properties of the filament should be designed for effortless processability. Polymer blending and the addition of excipients (non-organic fillers, plasticizers etc.) are a promising solution to reach desired mechanical and rheological properties (Aho et al., 2019; Fuenmayor et al., 2018).

Once the filament melts within the liquefier, it is deposited via a heated nozzle onto the print bed. Accuracy of material deposition defines the uniformity of the printing process which is crucial for the technology adoption. Material flow should be steady without potential air bubbles or nozzle clogging. Melt viscosity, printing temperature and filament thickness variation can all impact the quality of final dosage forms (Aho et al., 2019). Optimal printing temperature can be hard to determine. On one hand it is limited by high melt viscosity, while high temperatures can lead to drug and/or polymer degradation (Aho et al., 2019). Rheological properties of filaments are therefore crucial to assess the material's performance during material deposition. However, investigation into the uniformity of the 3D printed tablet's characteristics is largely neglected.

Filament formulation on can be a challenging process. Trial and error approach is wasteful, time-consuming and costly. Currently, there is no definitive filament property profile established, which would serve as a guidance for material selection and printability (Fuenmayor et al., 2018). Development of predictive models is necessary to facilitate the formulation process. In this way, filament composition could be improved not only to assure filament feedability, but also to promote the reproducibility of printed layers merging, thereby improving the uniformity of tablet properties to accommodate the pharmacopeial requirements for tablets.

A few mechanical screening techniques for filament formulation have already been introduced with a varying degree of success. The Zhang-Repka testing methodology features the use of a texture analyzer in a bending and indentation mode to assess brittleness, flexibility and stiffness of the filament specimen. By using the three-point bend test holder, the test is carried out on a short piece of the filament. The top blade either displaces or indents the filament, while force, and distance are measured (Zhang et al., 2019, 2017). Based on the observations, filaments with the following characteristics are processable: breaking distance > 0.61 mm, breaking stress > 635.5 g/mm^2 and stiffness > 20758.3 g/mm^2 (Zhang et al., 2019). Another screening compression test was developed with a texture analyzer where filament was mounted between two far-end caps. Force is recorded as the caps move towards one another and the measurements are characterized in feedable, tunable and non-feedable groups of filaments (Nasereddin et al.,

2018). Xu et al. tested both methods and the stiffness test appeared to be the most accurate screening technique. The stiffness threshold for printability was determined at 80 g/mm^2 (Xu et al., 2020). However, availability of various 3D printers and hardware make it hard to generalize a design space across all equipment (Henry et al., 2021). Bowden and direct extrusion FDM 3D printers certainly differentiate in filament requirements for processability, as the feeding process varies (Fuenmayor et al., 2018; Xu et al., 2020). Other mechanical and rheological tests (tensile strength, fracturability, melt flow indexing, complex viscosity etc.) are occasionally performed to explain certain filament characteristics (Fuenmayor et al., 2018; Gültekin et al., 2019; Henry et al., 2021; Samaro et al., 2020; Shi et al., 2021; Solanki et al., 2018; Than and Titapiwatanakun, 2021). However, a systematic approach to identify key filament properties is still lacking. As rheological and mechanical properties of filaments might impact not only the processability, but also the consistency of material deposition, consistency of interlayer merging and uniformity of tablet attributes, several filament properties were measured and correlated in this study. The aim of this article is therefore to identify key properties of filaments which are responsible for processability and the uniformity of the critical quality attributes of tablets.

Lastly, important novelty in *in silico* computational approaches to predict extrusion and printing temperatures, filament mechanical characteristics, printability and drug release of 3D printed tablets were achieved (Muñiz Castro et al., 2021; Ong et al., 2022). Input data was obtained from in-house measurements and extensive data mining of published literature. Filament composition, physical properties, equipment specifics and tablet design were considered to set predictive models with a high degree of accuracy. The open-access software M3DISEEN can be used in preliminary trials to screen a wide variety of formulations for printing suitability.

2. Materials and methods

2.1. Materials for extrusion

Active pharmaceutical ingredient ketoprofen and all other excipients were obtained internally from Lek pharmaceuticals d.d.. 12 pharmaceutical grade polymers were screened for printing suitability: Soluplus® (polyvinyl caprolactam–polyvinyl acetate–polyethylene glycol graft copolymer), Kollidon® 30 (polyvinylpyrrolidone), Kollidon® VA 64 (vinylpyrrolidone-vinyl acetate copolymer), Klucel™ EF (hydroxypropyl cellulose), Klucel™ LF (hydroxypropyl cellulose), Plasdone™ K-17 (polyvinylpyrrolidone), Plasdone™ K-25 (polyvinylpyrrolidone), Polyox™ WSR N750 (polyethylene oxide), Affinisol™ HPMC HME 15 LV (hydroxypropyl methylcellulose), Parteck® MXP (polyvinyl alcohol), Shin-Etsu AQOAT® AS-LG (hydroxypropyl methylcellulose acetate succinate) and Nisso HPC SSL (hydroxypropyl cellulose). Plasticizers Parteck® M200 (mannitol) or Polyglykol® 3350 P (polyethylene glycol) were introduced into certain physical mixtures to facilitate the extrusion process. To improve flowability of the powder blend, glidant Syloid® 244 FP (fumed silica) was added to all physical mixtures.

2.2. Hot-melt extrusion and filament preparation

All filaments were prepared in a single-screw full filament extrusion system Noztek Xcalibur (Noztek, Shoreham-by-Sea, UK). Elements of the single screw are fixed. Extruder consists of a

gravitational feeder, three heating zones and a 1.75 mm die. 1000 g of physical mixture were manually loaded into the feeder. Final composition of filaments was fixed to 20.0 % of ketoprofen, 0.5 % of Syloid 244 FP, 69.5 – 79.5 % of polymers and 0 – 10.0 % of plasticizers. The extrusion of each blend was carried out at different temperatures and screw speeds. Prepared materials were cooled by an air-cooling system. Filament thickness was controlled by a tolerance puller whose function is to pull the molten filament via a set of wheels out of the die. It contains a laser which measures the filament thickness in real time and the puller speed adjusts as necessary to maintain the set diameter in a feedback loop. Filaments with a 1.75 mm ± 0.05 mm diameter were collected on spools for subsequent 3D printing. Around 300 g of filaments were were collected and cut on the ZSE12 HP-PH (Leistritz Group, Nürnberg, Germany) strand cutter at 550 rpm to obtain pellet sized particles for subsequent rheological analysis.

During the study, filaments were stored in double PE bags, which were additionally sealed with aluminium bag. Pellets were stored in double PE bags and were rheologically analysed within a week. 3D printed tablets were stored in glass containers, which were sealed in aluminium bag. In this way, the prepared materials were protected from moisture uptake, thus filament and tablet qualities were not impacted by the environmental conditions.

2.3. Mechanical characterization of filaments

The nanoindentation test was used for determination of the sample indentation hardness (*H*) and elastic modulus (E_r). The tests were performed on the Nanoindenter G200 XP instrument manufactured by Agilent (Agilent Technologies, Inc, California, US). Continuous Stiffness Measurement (CSM) was performed using a standard three-sided pyramidal Berkovich probe with the tip oscillation frequency of 45 Hz and 2 nm harmonic amplitude. Sample filament granules obtained by strand cutter (Leistritz Group, Nürnberg, Germany) were put into a holder (placed on Teflon plate) with a diameter of 8 mm and height 1 mm, melted at the temperature of 3D printing for 10 minutes, pressure loaded with a 1 kg weight for another 10 minutes and then cooled down at air temperature. Each sample was probed with 20 indents with a 200 µm distance to exclude interaction effects. For the calculation of the elastic modulus and indentation hardness the values at the depths of 1000 nm and 1800 nm were used. All measurements were conducted at room temperature.

The fracture toughness was determined by using a three-point bending test, which was performed on dynamic mechanical analyser MCR702 (Anton Paar, Graz, Austria) with upper three-point bending tool and lower measurements sensor TPB 20 (measured at support distance length of 20 mm). The load was applied on the 3D printed filaments at room temperature and increased linearly from 0.01 to 10 N. Five repetitions were performed on each sample and the averaged values were used as a result.

The stiffness test was used to evaluate the resistance against microindentation as a measure of sample surface stiffness. Instron 3342 single column texture analyser (Instron, Massachusetts, USA) was used to perform the experiments with a 100 N maximum loading cell. The test was adapted to the machine and loading cell based on a previous publication (Zhang et al., 2019). The setup differs from the three-point bending test in terms of sample support during loading which

is represented by flat metal surface along the sample length. Filaments were cut into short extrudates of 3 cm and placed onto the metal surface. During testing, the probe slowly moved towards the sample with the speed of 0.5 mm/s until the surface of the extrudate was detected at the force of 0.05 N. At that point, the blade indented the samples with the speed of 2.0 mm/s until 0.4 mm indentation was reached and the required force for indentation was recorded. All experiments were performed in 10 replicates and results of average indentation forces were analysed in Bluehill 3 software (Instron, Massachusetts, USA). Force and extension data were collected at 200 points/second. Since all of the filaments were close to the 1.75 mm thickness, the surface area of penetration was not used for calculations and was deemed constant for all investigated samples.

2.4. Rheological characterization of filaments

Rheological measurements were performed in an inert nitrogen atmosphere with a rotational controlled rate rheometer MCR302 (Anton Paar, Graz, Austria). A plate-plate sensor system with a diameter of 25 mm (PP25) and a gap of 1 mm was used. The samples were directly placed on sensor system, which was preheated at the temperature of 3D printing for each sample. The filament sample's granules were put on the lower plate and heated at a constant temperature until the sample melted completely. At this time the upper plate was lowered to measuring gap dimension. The standard rotational flow tests were performed by changing the shear rate (ramp logarithmic) from 0.1 to 50 s^{-1} at the temperature of 3D printing corresponding to each sample. For further rheological characterization, the frequency, amplitude, and temperature dependent oscillatory sweep tests were performed. During the frequency tests, the dependence of the dynamic storage (*G'*) and loss (*G"*) modulus on the frequency was followed in the range between 0.1 and 100 Hz (ramp logarithmic) at a temperature of 3D printing corresponding to each sample. All tests were performed at constant shear strain 0.1 %, which was in the range of linear viscoelastic response. Amplitude tests were performed in the shear strain from 0.001 to 100 % (ramp logarithmic), constant frequency of 1 Hz and at the temperature of the 3D printing corresponding to each sample. In the temperature tests, which were performed at a constant frequency of 1 Hz, at constant shear strain 0.1 % and normal force 0 N, the temperature was changed at a rate of 2 °C/min in the temperature range between 70 °C and 250 °C, depending on the temperature of 3D printing for each sample and its composition. The rheological stability tests of the materials were performed at the temperature of 3D printing corresponding to each sample, at constant shear strain 0.5 % and frequency of 1 Hz in the duration time of 40 minutes.

2.5. 3D printing process

Capsule shaped tablets with 16.0 mm length, 7.0 mm thickness, 5.1 mm height and 1.5 mm fillet height were designed in SOLIDWORKS® 2018 (Dassault Systèmes, Massachusetts, USA). Designs were sliced and prepared for printing with Simplify3D® software (Simplify3D, Ohio, USA). 3D printing was performed in a custom-made 3D printer FDM-3P (Zavod 404, Ljubljana, Slovenia). Printing parameters were set at 50 % infill, 0.3 mm layer height, rectlinear infill pattern, 50 % outline overlap, one top and bottom layers, speed was set to 20 mm/s. Printing temperature varied based on the composition of the filaments. Printbed temperature was adapted to each

filament between 25 and 60 °C to achieve adequate adhesion between the printbed and the deposited material. Tablets were actively cooled during the printing process with external ventilators mounted to the printhead. 24 tablets per filament were printed in sequential mode for further analysis.

2.6. Tablet characterization

Tablets were analysed for dimensions, mass, mass uniformity, disintegration time and dissolution profile. Tablet dimensions were measured with a digital beak gauge (Unior d.d., Zrece, Slovenia) in 10 replicates. An average value and a relative standard deviation were calculated. Tablet mass was determined on an analytical scale (Sartorius AX224, Sartorius AG, Göttingen, Germany) in 10 replicates and an average mass and relative standard deviation were calculated. Disintegration study was performed with disks in Erweka ZT 304 disintegration tester (Erweka GmbH, Langen, Germany) according to the European Pharmacopoeia, 10th edition, 2020; 2.9.1. Disintegration of tablets and capsules in 6 replicates. An average value and a relative standard deviation were calculated. Dissolution tests were carried out in the Varian VK 7010 dissolution apparatus (Agilent Technologies, Inc, California, US) in a paddle configuration. Samples were placed in vessels containing 900 ml of the dissolution medium 0.05 M KH_2PO_4 phosphate buffer with pH 7.5. Due to low infill percentage, some tablets were freely floating in the dissolution medium. Therefore, in all cases metal sinkers were used to trap the tablets and prevent floating or sticking to the dissolution apparatus. The vessels were stirred at 100 rpm and the temperature of the dissolution medium was maintained at 37 ° C throughout the experiments. Aliquots of 5 ml were taken at 5, 10, 15, 20, 30, 45 and 60 minutes and filtered through 0.45 µm RC 25 mm filters (Lab Logistics Group International GmbH, Meckenheim, Germany). In cases when drug dissolution was not yet completed, additional aliquots were sampled after 120, 180, 240, 300, 360 and 420 minutes until complete release of ketoprofen. Sample absorbance was measured with Agilent 8453 UV/VIS spectrophotometer (Agilent Technologies, Inc, California, US) at 260 nm wavelength and a calibration curve was prepared (R^2 = 0.99950) in order to determine ketoprofen concentration. All samples were analysed in 6 replicates. An average value and relative standard deviation were calculated for each sampling point. Relative standard deviation of drug release was calculated when 60 % of ketoprofen was released, since RSD values were the highest for the majority of formulations at this point.

2.7. Statistical analysis

Minitab® 20 statistical software (Minitab LLC, Pennsylvania, USA) was used to perform the multiple linear regression (MLR). After preliminary studies, 15 variables (filament mechanical and rheological properties) were selected for final statistical modelling of 9 responses (filament processability, uniformity of tablet attributes). Each model was built with a stepwise selection approach, which continually adds and removes variables to and from the model to find a subset of variables leading to the best performing model in terms of model fit and predictive capability. Alpha to enter and alpha to remove variables from model were set to 0.15. Variables of tablet attributes were first standardized by subtracting the mean and dividing by standard deviation of each variable in order to reduce multicollinearity and compare the variables on a similar scale. K-

fold cross-validation method was performed to test each generated model with a number of folds set to 5. K-fold cross-validation is a common technique for validating predictive models. The dataset is divided into k subsets or folds (k = 5). The model is trained and evaluated k times, using a different subset of data as the validation set each time. Performance metrics from each fold are averaged to estimate the model's generalized performance. Before the MLR, normality of distribution of each response was checked and data were transformed accordingly with a Box-Cox transformation for mass uniformity (λ = - 0.5), diameter uniformity (λ = 0), height uniformity (λ = 0.5), width uniformity (λ = 0.5), drug release (λ = 0) and disintegration time (λ = 0). Additionally, assumptions of MLR were confirmed for all models (linearity, multicollinearity, homoscedasticity, multivariate normality, autocorrelation). Each model was evaluated based on the coefficients of determination R^2, R^2 adjusted, R^2 predicted and 5-fold R^2 (after validation).

3. Results and discussion

3.1. Filament formulation and material characterization

Fused deposition modelling is a complex technology when it comes to filament formulation approach. Filaments require excellent mechanical and rheological properties, while also thermal stability of components should be established. For this purpose, a wide variety of pharmaceutical grade polymers were screened for 3D printing suitability. Filament compositions were adjusted accordingly to obtain a broad span of filaments, ranging from very brittle, to optimal to very pliable. In this way, a wide range of possible filaments was covered which is beneficial for the predictability of the statistical models. Final composition of filaments (Table 1) was fixed to 20.0 % of ketoprofen, 0.5 % of Syloid 244 FP, 69.5 – 79.5 % of polymers and 0 – 10.0 % of plasticizers. After preliminary extrusion testing, 23 filament formulations were extruded and processability of filaments was determined by employing FDM 3D printing process (Table 1).

The feeding mechanism of FDM-3P printer firmly pushes the filament through the liquefier. When printing with 0.3 mm nozzle size, the shear rate acting on the filament is $\dot{\gamma}$ = 363 s^{-1}. Filaments could become easily damaged by the drive and pinch wheel in absence of suitable mechanical properties. In addition, the rheological properties of the molten filaments should be adequate for exact and repeatable material deposition. This is achieved in part by adjusting the temperature of the heated nozzle accordingly, usually above the extrusion temperature (Parulski et al., 2021; Pietrzak et al., 2015). In this series of experiments, the difference between the printing and extrusion temperature for different filaments ranged between 0 and 65 ° C, contributing to a wide span of possible rheological properties.

Table 1 Composition of filaments, extrusion conditions and printing temperature

Powder Blend	Substance	Composition	Extrusion temperature [°C]			Screw Speed	Printing temperature
		(%)	Z1	Z2	Z3	rpm	[°C]
M1	Affinisol™ HPMC HME 15 LV	69.5	60	145	145	10	210
	Ketoprofen	20.0					
	Parteck® M200	10.0					
	Syloid® 244 FP	0.5					
M2	Parteck® MXP	69.5	50	170	170	18	190
	Ketoprofen	20.0					
	Parteck® M200	10.0					
	Syloid® 244 FP	0.5					
M3	Soluplus®	69.5	75	115	115	22	150
	Ketoprofen	20.0					
	Parteck® M200	10.0					
	Syloid® 244 FP	0.5					
	Shin-Etsu AQOAT® AS-LG	69.5					

M4	Ketoprofen	20.0	90	140	140	25	150
	Parteck® M200	10.0					
	Syloid® 244 FP	0.5					
M5	Soluplus®	79.5	70	130	130	15	130
	Ketoprofen	20.0					
	Syloid® 244 FP	0.5					
M6	Shin-Etsu AQOAT® AS-LG	79.5	90	145	145	10	165
	Ketoprofen	20.0					
	Syloid® 244 FP	0.5					
M7	Parteck® MXP	79.5	80	188	188	13	200
	Ketoprofen	20.0					
	Syloid® 244 FP	0.5					
M8	Kollidon® 30	34.75	100	145	145	13	165
	Polyox™ WSR N750	34.75					
	Ketoprofen	20.0					
	Parteck® M200	10.0					

	Syloid® 244 FP	0.5					
M9	Affinisol™ HPMC HME 15 LV	39.5	65	150	150	15	150
	Kollidon® VA 64	30.0					
	Ketoprofen	20.0					
	Parteck® M200	10.0					
	Syloid® 244 FP	0.5					
M10	Affinisol™ HPMC HME 15 LV	59.5	65	150	150	17	190
	Kollidon® VA 64	10.0					
	Ketoprofen	20.0					
	Parteck® M200	10.0					
	Syloid® 244 FP	0.5					
M11	Nisso HPC SSL	39.5	50	130	130	13	145
	Plasdone™ K-25	30.0					
	Ketoprofen	20.0					
	Parteck® M200	10.0					
	Syloid® 244 FP	0.5					

M12	Klucel™ LF	30.0	70	140	140	9	170
	Kollidon® 30	39.5					
	Ketoprofen	20.0					
	Parteck® M200	10.0					
	Syloid® 244 FP	0.5					
M13	Klucel™ EF	20.0	60	135	135	10	160
	Kollidon® VA 64	49.5					
	Ketoprofen	20.0					
	Parteck® M200	10.0					
	Syloid® 244 FP	0.5					
M14	Klucel™ EF	39.5	65	135	135	10	170
	Kollidon® VA 64	30.0					
	Ketoprofen	20.0					
	Parteck® M200	10.0					
	Syloid® 244 FP	0.5					
	Klucel™ EF	30.0					
	Plasdone™ K-17	39.5					

M15	Ketoprofen	20.0	60	125	125	10	145
	Parteck® M200	10.0					
	Syloid® 244 FP	0.5					
M16	Kollidon® 30	20.0	60	145	145	6	170
	Polyox™ WSR N750	49.5					
	Ketoprofen	20.0					
	Parteck® M200	10.0					
	Syloid® 244 FP	0.5					
M17	Klucel™ LF	49.5	65	140	140	7	180
	Kollidon® 30	20.0					
	Ketoprofen	20.0					
	Parteck® M200	10.0					
	Syloid® 244 FP	0.5					
M18	Kollidon® VA 64	69.5	50	95	95	16	120*
	Ketoprofen	20.0					
	Polyglykol® 3350 P	10.0					
	Syloid® 244 FP	0.5					

M19	Soluplus®	69.5	95	105	105	18	150*
	Ketoprofen	20.0					
	Polyglykol® 3350 P	10.0					
	Syloid® 244 FP	0.5					
M20	Plasdone™ K-25	69.5	50	125	125	15	145*
	Ketoprofen	20.0					
	Polyglykol® 3350 P	10.0					
	Syloid® 244 FP	0.5					
M21	Shin-Etsu AQOAT® AS-LG	69.5	50	140	140	29	145*
	Ketoprofen	20.0					
	Polyglykol® 3350 P	10.0					
	Syloid® 244 FP	0.5					
M22	Kollidon® 30	69.5	60	135	135	14	160*
	Ketoprofen	20.0					
	Parteck® M200	10.0					
	Syloid® 244 FP	0.5					

M23	Klucel™ EF	69.5	60	115	115	6	150*
	Ketoprofen	20.0					
	Parteck® M200	10.0					
	Syloid® 244 FP	0.5					

*printing temperature assessed by manual feeding, as the filaments were not processable

17 filaments were printable (M1 – M17), while 6 were not processable due to high brittleness or pliability (M18-M23). Nevertheless, not many filaments were able to pass the printhead without the polymer mixing approach. Affinisol™ HPMC HME 15 LV, Parteck® MXP, Shin-Etsu AQOAT® AS-LG and Soluplus® were the only polymers with adequate properties for printing with (M1 – M4) or without (M5 – M7) plasticizer presence. Apart from Soluplus®, these findings are in line with the published literature (Crișan et al., 2021; Goyanes et al., 2017; Prasad et al., 2019). It has been reported, that Soluplus® is too brittle for feeding (Alhijjaj et al., 2016; Henry et al., 2021). While the brittle nature of Soluplus® was observed, the filaments did not break during the printing process. This discrepancy highlights the importance of specific equipment design in 3D printers as the processability of certain filaments can depend on the selected 3D printer. On the other hand, it could be that the drug ketoprofen might have a small plasticizing effect, which prevented the filament breakage.

No other filaments composed of a single polymer, were able to cross the printhead without breakage or buckling. Kollidon® 30, Kollidon® VA 64, Plasdone™ K-25 and Plasdone™ K-17 were all too brittle and became quickly damaged by the feeding mechanism. Regardless of the grade, polyvinyl pyrrolidone could not resist the breakage due to high pressure of the feeding mechanism. Polyox™ WSR N750, Nisso HPC SSL, Klucel™ LF and Klucel™ EF were too soft and pliable for printing. In combination with the drug, plasticizer and glidant, they have all quickly jammed the 3D printer. However, a combination of a brittle polymer with high column strength and a pliable filament without breaking issues can yield a suitable printing formulation as each polymer cancels out the mechanical disadvantages of the other polymer in the filament. This was definitely the case for filaments M8 – M17. For example, it was demonstrated that a mere 20 % addition of a flexible polymer to a brittle filament changes the behaviour of a brittle formulation towards a printable one (M13). A similar conclusion was reached for pliable formulations, where a 20 % addition of a brittle polymer reduced the soft filament character, resulting in a feedable filament (M16, M17). Therefore, polymer mixing represents an exciting formulation approach to improve the processability of filaments with a proposed limit of 20 % as a minimum quantity of a mechanically complementary polymer.

Filaments M18 – M23 were not processable due to high brittleness, pliability or even both. Formulations M20 and M22 were broken by the feeding mechanism, while M19, M21 and M23 jammed the 3D printer due to the buckling phenomena. M18 demonstrated both troublesome qualities. Plasticizer Polyglykol® 3350 P also displayed poor qualities as an additive due to excessive softening of the filaments. 10 % of Polyglykol® 3350 P was added to the otherwise printable formulations containing either polymer Soluplus® (M19) or Shin-Etsu AQOAT® AS-LG (M21) with the purpose of reducing the extrusion and printing temperature. However, Polyglykol® 3350 P softened the filaments to a high extent, leading to extreme pliability and flexibility. The same conclusion was reached for M18 which is composed of a brittle polymer Kollidon® VA 64. While the brittle character did not appear to improve, additional flexibility yielded an especially unprocessable filament. Polyglykol® 3350 P might therefore be a less suitable plasticizer for the 3D printing purposes. While the extrusion temperature can be reduced, the filament characteristics are not appropriate for 3D printing. It could also be that a 10 % addition of Polyglykol® 3350 P was excessive and smaller amounts might lead to a better filament. In addition, other polyethylene glycol grades, such as PEG 6000, might be more useful for the plasticizing purpose (Isreb et al., 2019; Kempin et al., 2018).

Once the filaments and 3D printed tablets were successfully prepared, an in-depth study into filament and tablet characterization was performed. A wide array of filament properties was gathered from mechanical and rheological analysis. Elastic modulus (E_r), indentation hardness (H), flexural stress (σ_f), surface stiffness (S) and relative standard deviation of surface stiffness ($SRSD$) were obtained as a result of mechanical tests, while rheological tests yielded melt viscosity (η) taken at different shear rates (0.106 s^{-1}, 10 s^{-1} and 47 s^{-1}), storage modulus (G'), loss modulus (G'') and loss factor ($tan\ \delta$) in temperature sweep mode at printing temperature and storage modulus (G'), loss modulus (G'') and loss factor ($tan\ \delta$) in amplitude and frequency sweep mode taken at different shear strains (1 % and 68.5 %) or frequencies (0.121 Hz, 3 Hz and 82.5 Hz) (Table 2, Table 3). In addition, standard tablet characterization was performed. Analysis comprised of uniformity of mass, uniformity of dimensions, drug release, uniformity of drug release, disintegration time and uniformity of disintegration time (Table 4).

A preliminary MLR analysis between filament properties, processability and tablet properties was conducted in order to separate the filament properties to the correlating (Table 2) and non-correlating ones (Table 3). This was done in an attempt to limit the amount of input variables and reduce the complexity of the statistical modelling while retaining the important correlating filament properties. 15 input variables were used in the final statistical modelling (Table 2).

Table 2 Mechanical and rheological properties of filaments M1 – M23, which were successfully correlated to processability and/or tablet properties using multiple linear regression.

term	T_p	*tan δ*	*G''*	*η*	*tan δ*	*G'*	*tan δ*	*G''*	*tan δ*	*tan δ*	E_r	*H*	σ_f	*S*	*SRSD*
(taken at)	/	($T=T_p$)	($T=T_p$)	($\dot{\gamma}$=10 s^{-1}) [Pa·s]	(f=56 Hz)	(f=56 Hz)	(f=3 Hz)	(f=82.5 Hz)	(f=0.12 Hz)	(γ=68.5 %)	(1 µm)	(1.8 µm)	(2.5 % defl) [MPa]	(0.4 mm)	/
[unit]	[°C]	/	[Pa]		/	[Pa]	/	[Pa]	/	/	[GPa]	[GPa]		[N]	[%]
M1	210	3.29	2329.00	36.29	1.65	12910.00	2.65	24969	2.47	5.97	1.54	0.04	20.76	54.18	5.59
M2	190	2.37	729.03	81.21	5.74	1972.10	4.67	12999	2.35	9.30	3.82	0.07	30.16	58.13	19.14
M3	150	6.53	1173.40	95.63	2.21	9772.40	4.47	26790	2.87	9.47	3.59	0.11	8.75	46.09	30.26
M4	150	1.04	29704.00	3331.10	0.65	227300.00	0.91	165980	1.22	1.31	3.82	0.06	67.43	63.88	28.40
M5	130	2.43	15397.00	1456.50	1.19	108410.00	1.85	157100	5.23	3.02	2.85	0.12	12.66	56.46	21.37
M6	165	1.06	20880.00	3445.30	0.76	72802.00	1.06	61709	1.31	1.31	3.66	0.14	56.07	65.44	12.87
M7	200	4.25	2691.50	94.84	3.55	3753.90	4.50	10688	2.01	7.79	6.04	0.27	30.15	78.65	3.48
M8	165	1.62	12682.00	1057.70	0.73	56931.00	1.15	41364	2.40	2.35	2.59	0.12	0.00	57.28	8.65
M9	150	1.00	9068.20	276.13	0.83	91389.00	0.75	89765	0.77	4.50	4.06	0.18	10.33	46.83	11.61

M10	190	1.13	6135.50	20.39	0.66	44187.00	1.07	30068	1.67	2.82	2.69	0.09	26.32	58.70	13.59
M11	145	3.36	2019.30	411.55	1.28	54306.00	3.17	80291	6.69	6.56	3.97	0.14	14.11	54.32	15.58
M12	170	1.01	1819.00	32.17	0.81	18718.00	1.14	11638	1.63	1.60	2.94	0.10	40.84	70.13	10.62
M13	160	1.99	448.14	27.59	1.74	5729.30	3.15	10951	5.16	5.40	3.88	0.14	36.11	37.77	22.29
M14	170	2.91	431.70	43.40	1.76	6909.00	2.93	11709	4.13	5.50	2.56	0.06	29.71	63.30	16.13
M15	145	1.61	8528.20	249.40	0.83	37937.00	1.37	37739	3.90	2.33	3.61	0.13	13.82	43.53	27.65
M16	170	1.08	27221.00	914.59	0.55	148510.00	0.94	88046	1.85	1.53	1.32	0.01	23.64	32.25	15.47
M17	180	1.21	6947.80	8.58	0.76	21155.00	1.19	15302	1.85	2.00	2.06	0.05	41.12	38.94	16.41
M18	120	7.98	4075.00	132.75	3.89	8190.70	8.22	41499	16.66	12.74	1.91	0.04	0.00	12.74	32.27
M19	150	3.16	111.28	41.16	4.86	1344.00	4.76	8693	4.31	12.58	0.54	0.00	0.00	29.54	26.09
M20	145	3.38	1522.50	6.74	2.42	15280.00	3.38	39924	5.23	5.64	4.35	0.22	0.00	10.98	17.85
M21	145	1.21	14070.00	2050.40	0.76	55820.00	1.10	44594	1.57	1.57	1.28	0.02	7.79	30.42	15.09
M22	160	1.96	1494.00	99.91	1.52	13382.00	2.21	20426	2.14	2.31	4.49	0.21	0.00	26.08	51.12
M23	150	1.45	8184.50	104.96	0.56	92977.00	1.06	56759	2.53	2.00	0.15	0.00	3.90	9.50	11.70

Table 3 Mechanical and rheological properties of filaments M1 – M23 with identified absence of correlation to processability and tablet properties as concluded after preliminary multivariant analysis.

term (taken at) [unit]	*G'* ($T=T_p$) [Pa]	*η* ($\dot{\gamma}$=0.11 s^{-1}) [Pa·s]	*η* ($\dot{\gamma}$=47 s^{-1}) [Pa·s]	*G''* (f=56 Hz) [Pa]	*G'* (f=3 Hz) [Pa]	*G''* (f=3 Hz) [Pa]	*tan δ* (f=82.5 Hz) /	*G'* (f=82.5 Hz) [Pa]	*G'* (f=0.12 Hz) [Pa]	*G''* (f=0.12 Hz) [Pa]	*tan δ* (γ=1 %) /	*G'* (γ=1 %) [Pa]	*G''* (γ=1 %) [Pa]	*G'* (γ=68.5 %) [Pa]	*G''* (γ=68.5 %) [Pa]
M1	707.85	386.95	0.05	21357	1385.30	3664.20	2.84	8785.70	68.48	168.99	3.79	285.45	1082.00	137.91	823.52
M2	307.53	315.77	0.46	11311	304.15	1419.10	19999.69	0.65	48.05	113.11	9.36	63.00	589.94	63.83	593.47
M3	179.64	192.70	0.72	21554	561.56	2508.00	2.63	10171.00	58.84	168.71	5.10	185.88	947.28	91.06	862.53
M4	28535.00	43949.00	2459.10	148030	61473.00	55791.00	0.63	262390.00	9957.20	12136.00	1.04	32240.00	33437.00	18806.00	24670.00
M5	6347.80	3366.60	755.47	128600	14577.00	26982.00	1.18	133610.00	427.72	2237.20	2.68	4135.20	11080.00	3302.40	9960.50
M6	19641.00	30694.00	2215.30	55299	18078.00	19085.00	0.75	82055.00	3311.50	4346.70	1.16	9826.60	11409.00	6575.50	8638.30

M7	633.42	298.71	16.32	13335	339.19	1526.10	31.71	337.03	56.92	114.40	3.95	149.07	588.81	92.53	721.09
M8	7828.20	6034.70	401.92	41794	12901.00	14868.00	0.63	65264.00	1153.40	2767.00	1.50	6099.10	9151.30	1967.70	4618.80
M9	9056.70	10081.00	87.23	75914	28916.00	21679.00	0.84	106900.00	8441.30	6526.10	0.90	15754.00	14249.00	916.46	4122.40
M10	5411.10	2599.00	7.19	28972	9906.70	10614.00	0.60	49736.00	979.29	1631.20	1.44	5276.90	7582.00	1371.50	3863.40
M11	601.83	971.88	171.92	69405	3630.70	11525.00	1.16	69039.00	101.23	677.00	5.34	573.54	3061.80	430.17	2823.70
M12	1808.00	1445.70	16.89	15080	4295.00	4903.80	0.60	19325.00	601.74	979.18	1.32	2508.20	3308.50	1581.60	2529.60
M13	225.55	85.53	0.00	9956	501.10	1578.50	2.64	4140.90	21.41	110.48	4.02	175.64	705.57	124.01	669.30
M14	148.26	230.68	0.00	12153	787.15	2307.60	4.19	2796.20	37.43	154.74	4.05	240.13	973.34	156.48	860.18
M15	5291.50	1760.10	77.26	31593	7039.60	9657.90	0.84	45176.00	263.12	1026.50	1.89	2998.60	5656.30	1650.40	3852.70
M16	25097.00	17466.00	161.19	82126	41496.00	39131.00	0.53	165340.00	4070.90	7532.30	1.24	19998.00	24869.00	9302.10	14223.00
M17	5764.90	1479.70	3.71	16070	5001.20	5937.60	0.78	19513.00	517.43	956.75	1.41	2433.50	3434.00	1037.70	2077.70

M18	510.55	163.38	93.76	31851	343.42	2821.50	5.81	7139.30	8.35	139.13	10.05	95.47	959.76	75.52	962.36
M19	35.16	70.67	26.11	6537	137.46	653.69	20000.00	0.43	11.96	51.50	10.21	15.07	153.75	12.07	151.93
M20	450.99	389.90	0.12	37000	1594.10	5392.40	3.05	13099.00	103.13	539.84	4.02	661.02	2657.10	128.59	725.15
M21	11589.00	18031.00	663.15	42409	13197.00	14446.00	0.70	63539.00	2163.40	3404.80	1.23	8547.80	10532.00	4360.50	6857.50
M22	763.42	729.92	72.61	20337	1637.10	3622.80	1.43	14286.00	204.27	436.64	2.30	817.64	1883.40	955.67	2210.30
M23	5639.70	7405.90	3.12	51927	24993.00	26574.00	0.56	102110.00	1570.80	3977.10	1.47	11400.00	16760.00	4349.70	8698.10

Table 4 Results of tablet characterization. NA represents data which is not available in case of tablets that did not disintegrate after 24 hours or due to non-feedable nature of filaments.

Filament	Processability 0=NO 1=YES	Mass RSD [%]	Tablet length RSD [%]	Tablet height RSD [%]	Tablet width RSD [%]	Time to 60 %	RSD of time to 60 %	Disintegration 0=NO	Disintegration time [min]	RSD of disintegration time [%]

						drug release [min]	release [%]	1=YES		
M1	1	4.53	0.78	1.77	0.44	107.33	42.30	1	446.17	23.63
M2	1	1.42	1.70	1.98	2.11	27.17	22.08	1	105.00	3.01
M3	1	3.51	1.17	2.28	2.99	127.17	32.14	0	NA	NA
M4	1	2.86	1.79	0.62	0.78	67.83	37.48	0	NA	NA
M5	1	2.56	0.95	1.06	1.14	266.25	36.40	0	NA	NA
M6	1	1.44	0.67	1.31	2.34	106.33	55.60	0	NA	NA
M7	1	2.63	1.20	0.83	1.37	45.92	18.24	1	129.17	11.48
M8	1	3.93	0.75	1.07	0.86	20.08	23.23	1	26.33	5.72
M9	1	4.32	0.96	3.95	0.64	25.67	24.64	1	54.17	19.93
M10	1	3.38	0.65	3.38	1.19	92.17	27.54	1	20.17	15.18
M11	1	4.28	1.01	1.99	4.13	15.04	32.27	1	34.83	21.59
M12	1	3.73	2.19	5.49	3.95	77.08	9.97	1	52.50	2.89

M13	1	2.47	1.20	3.19	3.78	27.33	12.70	1	38.83	6.80
M14	1	12.29	2.53	3.12	5.58	33.67	33.63	1	38.00	6.23
M15	1	5.07	1.90	3.68	3.88	34.33	4.39	1	46.17	5.72
M16	1	3.71	0.78	1.60	0.96	40.83	31.67	1	37.74	29.21
M17	1	6.17	0.94	1.22	1.49	86.58	7.30	1	60.42	16.32
M18	0	NA	NA	NA	NA	NA	NA	NA	NA	NA
M19	0	NA	NA	NA	NA	NA	NA	NA	NA	NA
M20	0	NA	NA	NA	NA	NA	NA	NA	NA	NA
M21	0	NA	NA	NA	NA	NA	NA	NA	NA	NA
M22	0	NA	NA	NA	NA	NA	NA	NA	NA	NA
M23	0	NA	NA	NA	NA	NA	NA	NA	NA	NA

3.2. Modelling of filament processability

Based on the measured mechanical and rheological properties of filaments, a statistical model was established with an above-described MLR method to identify key filament properties assuring feedability and to predict processability for future formulations based on the aforementioned measurements. The sample pool was composed of 17 printable (M1 – M17) and 6 unprintable (M18 – M23) filaments. A numeric value for processability was assigned to each filament, 1 in case of successful printing and 0 in case of filament breakage or pliability. 15 variables were correlated with processability.

A well-fitting model with good predictability was obtained, processability was well explained and predicted (R^2 = 0.74, $R^2_{(adj)}$ = 0.71, $R^2_{(pred)}$ = 0.67, $R^2_{(5\text{-fold})}$ = 0.70). Only the filament surface stiffness, measured with the Zhang-Repka methodology, and its square term defined the printability of the filaments (Fig. 1). Stiffness is defined as a ratio of load and deformation (Zhang et al., 2019). The recorded load force was directly proportional to the stiffness of the filament, as deformation was kept constant at 0.4 mm penetration depth into the filament. In addition, the filament diameter was constant among all formulations at 1.75 ± 0.05 mm. During the stiffness test, the probe indents the filament sample and imitates the feeding mechanism of the printhead. High measured forces indicate satisfactory resistance to surface damage during feeding, while low forces can point to poor feedability. Filaments with low surface stiffness are either too brittle and prone to breakage during the printing process or too soft and therefore pliable leading to buckling issues (Zhang et al., 2019). It was also observed, that brittle filaments broke at higher indentation depths (>0.6 mm), while pliable filaments did not reach surface stiffness comparable to printable filaments even at depths above 1.0 mm. This observation is in line with the published literature (Zhang et al., 2019). A rather low 0.4 mm distance was selected as final indentation depth where load force was recorded, since the maximum load of the measuring cell (100 N) was already reached at that distance for filaments with high surface stiffness.

It can be concluded, that the higher the stiffness of the filament, the better the printability. The applicability of the stiffness test is a desirable outcome, as a simple mechanical test can determine whether the filament suffers from excessive brittle or pliable character immediately after the filament extrusion process. In this way, filament feedability can be easily improved through formulation studies aimed at increasing the filament stiffness and avoiding the filament feeding issues. Previous studies already proved that the filament stiffness is indicative of processability (Xu et al., 2020; Zhang et al., 2019). However, the statistical model shows that the square term of stiffness is equally important. Additionally, the relationship between the filament stiffness and processability was confirmed on a wide variety of filaments composed of several polymers.

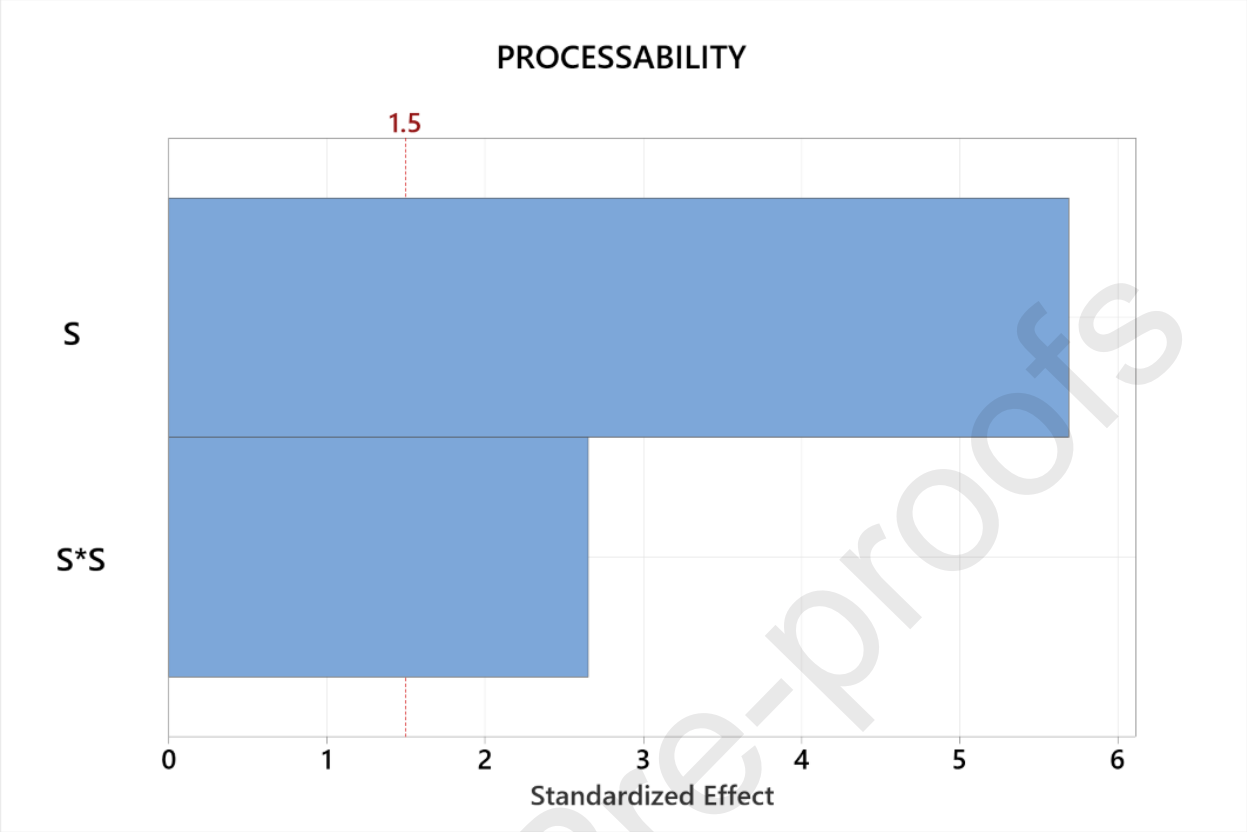

Fig. 1. Pareto chart for filament processability parameter, showing that only surface stiffness (*S*) and its square term (*S*S*) enter the model and determine printability.

Processability index (PI) is proposed as an estimate of filament feedability based on the Model Equation 1.

$$PI = -0.601 + 0.0485 \times S - 0.000356 \times S^2 \quad (1)$$

where PI is processability index, S is filament surface stiffness and S^2 is a square term of filament surface stiffness.

PI is defined as a value between 0 and 1, where 1 indicates a feedable character of filaments while 0 demonstrates non-feedable features, such as excessive brittleness of pliability. PI was calculated and assigned to each studied filament (Fig. 2). Indeed, the overlap between the observed processability and calculated processability index was evident for both groups of filaments (Fig. 2). Non-feedable filaments demonstrate a PI lower or equal to 0.54, while majority of feedable filaments provide PI values greater or equal to 0.72. The only borderline filament was M16, which despite being feedable in nature, is closer to the non-feedable group of filaments with PI = 0.59. It was noticed during 3D printing, that M16 filament was quite pliable in nature. Therefore, a cut-off value to designate feedable filaments was determined at PI = 0.72 to confidently establish an area of feedability despite neglecting some potentially borderline

feedable filaments. In other words, any filament with a PI greater or equal to 0.72 can be claimed as printable, while filaments with a PI lower or equal to 0.54 will not be processable. Filaments between both values can be designated as borderline feedable and additional studies are needed to accurately set the PI limits. However, these values are equipment-specific and are with certainty only valid for 3D printer FDM 3-P. Other printheads, regardless of the direct or bowden extrusion setup, can be composed of different elements and feed filaments under various mechanisms and settings, therefore the same limit cannot be applied. However, using the presented methodology, a similar experiment can be performed to establish a cut-off value for any model of the FDM 3D printer.

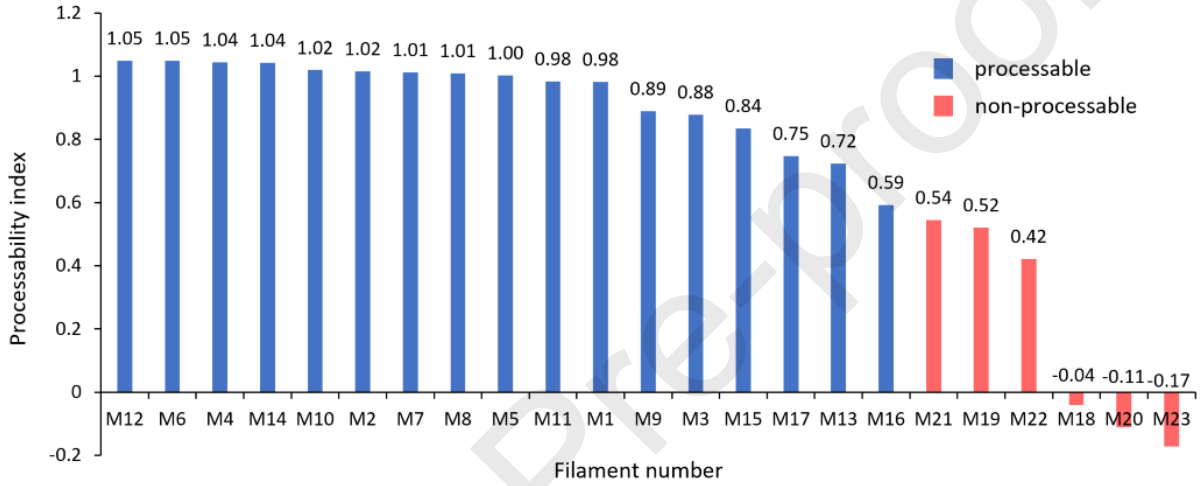

Fig. 2. Processability index calculated from model equation. Values towards 1 indicate a feedable filament character, while values close to 0 designate non-feedable filaments. Blue bars demonstrate processable filaments, while red bars label non-processable filaments as established through FDM 3D printing experiments.

3.3. Modelling of critical quality attributes of 3D printed tablets

Mechanical and rheological properties of filaments impact the uniformity of material deposition during the 3D printing process and uniformity of interlayer porosity. Mechanical properties define the reproducibility of the filament feeding rate with inconsistencies such as filament slipping. Once the filament is molten, the rheological properties of the material determine the consistency of material flow through the printer nozzle and the consistency of the tablet interlayer merging. Both properties determine the uniformity of the tablet formation process. Therefore, tablet mass uniformity, tablet dimensions uniformity, drug release extent, drug release uniformity, occurrence of disintegration, disintegration time and disintegration time uniformity were correlated with filament properties to identify key filament characteristics. In

this way, the filaments could be analysed mechanically and rheologically prior to printing trials in order to assess their suitability for printing from the point of view of the uniformity of the tablet properties.

The number of data instances was reduced for this part of study, as tablets were successfully prepared from only 17 filaments (M1 – M17). 15 filament mechanical and rheological variables were correlated to 8 critical quality attributes of tablets. A model was claimed as useful only in case of predicting at least 50 % of values of tablet properties ($R^2_{(pred)} > 0.50$). A well-fitting model with good predictability was obtained for the tablet width uniformity ($R^2 = 0.90$, $R^2_{(adj)} = 0.85$, $R^2_{(pred)} = 0.68$, $R^2_{(5\text{-fold})} = 0.69$), the drug release uniformity ($R^2 = 0.88$, $R^2_{(adj)} = 0.82$, $R^2_{(pred)} = 0.79$, $R^2_{(5\text{-fold})} = 0.73$), the occurrence of tablet disintegration ($R^2 = 0.83$, $R^2_{(adj)} = 0.79$, $R^2_{(pred)} = 0.64$, $R^2_{(5\text{-fold})} = 0.57$) and the disintegration time uniformity ($R^2 = 0.82$, $R^2_{(adj)} = 0.76$, $R^2_{(pred)} = 0.67$, $R^2_{(5\text{-fold})} = 0.61$) (Fig. 3). These well performing models are discussed in more detail in the next sections, although explaining the individual contributions of filament properties using Pareto charts is difficult due to the high complexity of the models (Fig. 4).

On the other hand, models with poor predictability were attained for the tablet mass uniformity ($R^2 = 0.61$, $R^2_{(adj)} = 0.56$, $R^2_{(pred)} = 0.30$, $R^2_{(5\text{-fold})} = 0.17$), the tablet length uniformity ($R^2 = 0.60$, $R^2_{(adj)} = 0.47$, $R^2_{(pred)} = 0.25$, $R^2_{(5\text{-fold})} = 0.24$), the tablet height uniformity ($R^2 = 0.61$, $R^2_{(adj)} = 0.52$, $R^2_{(pred)} = 0.37$, $R^2_{(5\text{-fold})} = 0.30$) and the tablet disintegration time ($R^2 = 0.70$, $R^2_{(adj)} = 0.64$, $R^2_{(pred)} = 0.47$, $R^2_{(5\text{-fold})} = 0.46$) (Fig. 3). Lastly, model for the drug release could not be established, as none of the measured filament properties correlated with the drug release profile. Further research is needed to uncover relationships between overlooked filament properties, tablet design, or printing parameters and critical tablet quality attributes with poorly performing models.

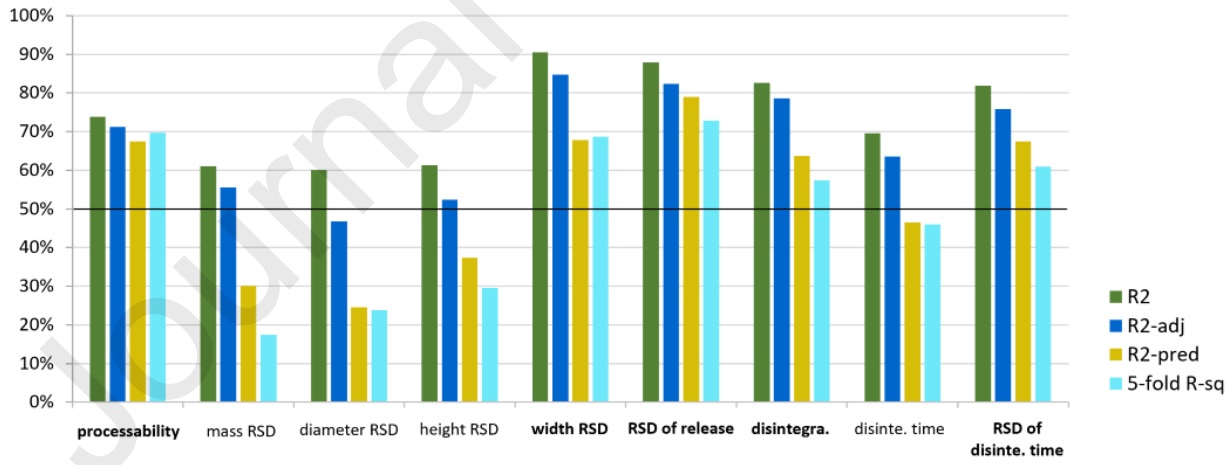

Fig. 3. Summary of fit plot representing models of filament processability, tablet mass uniformity, length, height and width uniformity, uniformity of drug release, occurrence of tablet disintegration, tablet disintegration time and its uniformity. Models with good predictability are labeled in bold, while the black line shows the cutoff limit of $R^2_{(pred)} = 0.50$.

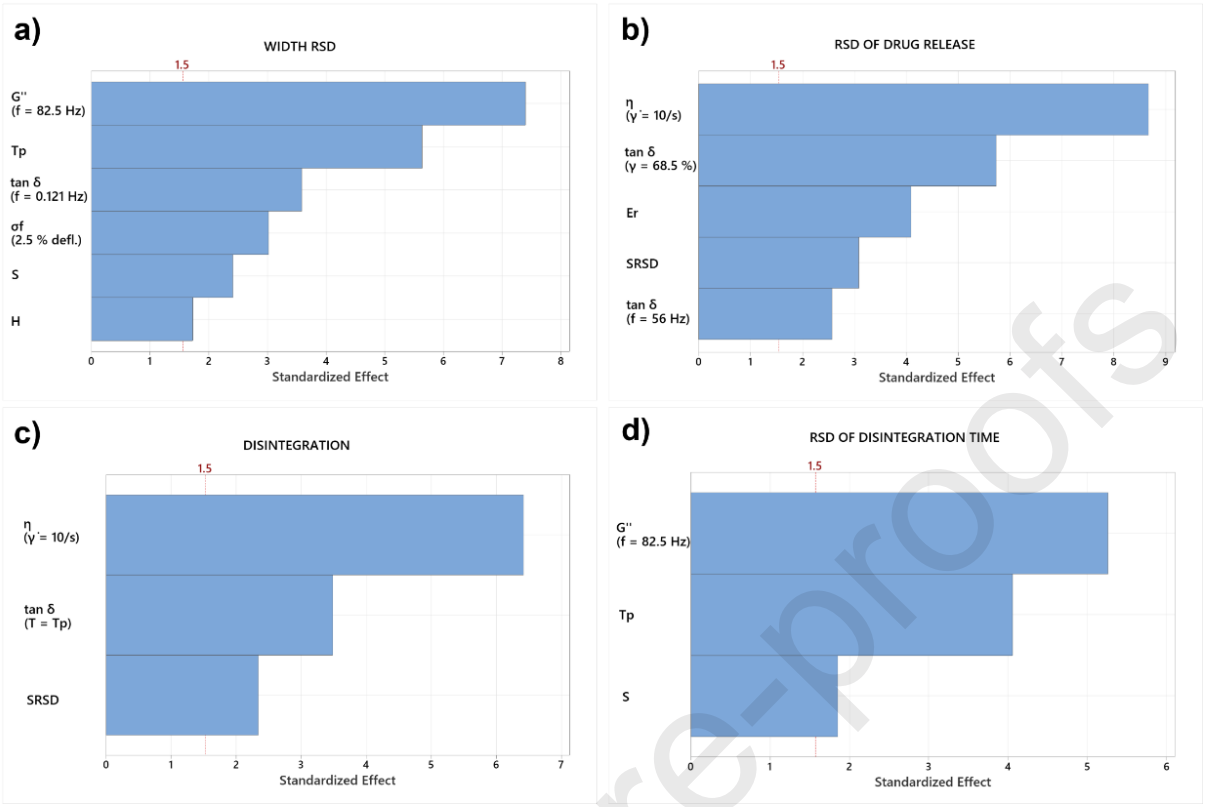

Fig. 4. Pareto charts of tablet width uniformity **(a)**, drug release uniformity **(b)**, tablet disintegration occurrence **(c)** and disintegration time uniformity **(d)** showing which filament properties form each predictive model. Blue bars indicate how much each variable influences investigated tablet property. The larger the bar of the model variable, the more pronounced is its influence on the tablet property. *G''* is filament loss modulus, *Tp* is printing temperature, *tan δ* is filament loss factor, σ_f its flexural stress, *S* its surface stiffness, *H* its hardness, *η* its melt viscosity, E_r its elastic modulus and *SRSD* is the relative standard deviation of filament surface stiffness.

3.3.1. Uniformity of tablet width

In general, the variability of tablet dimensions exceeded that of conventionally pressed tablets. Large inconsistencies (RSD > 5 %) in tablet height and width were observed for formulations M12 and M14 respectively (Table 4). High dimension RSD values for these two filaments could be partly explained by poor mass uniformity (3.73 % and 12.29 %) as a result of variable material mass flow during the printing process. On the other hand, deviations in dimensions can be expected to an extent, as dimensions of 3D printed tablets cannot be as uniform as traditionally compressed tablets. Normally, the die and punches of the tablet press regulate the tablet dimensions with deviations due to material elastic relaxation. In contrast, the dimensions of 3D printed tablets are determined by the CAD design and by the properties of the filaments, as polymers can expand or shrink during the melting and cooling process. The tablet's dimensions

uniformity can also be interpreted as filament's ability to consistently and evenly deposit and fuse in layers during the printing process. Both mechanisms can lead to inconsistencies in tablet dimensions.

Discrepancies in tablet length did not occur to the same relative extent due to the design of the 3D printed tablet. Tablet width is more than two times shorter compared to tablet length. In this way, deviations may be, assuming the same printing error, more noticeable along the shorter axis resulting in larger RSD values (2.21 % on average). Contrary, printing errors which can add or subtract along tablet length might not be as evident, since this dimension is longer (RSD 1.25 % on average). Tablet height, which is more comparable to tablet width in absolute term appears to have a similar inconsistency (RSD 2.26 % on average) when compared to tablet width.

Among the tablet dimensions, a good predictive model was obtained only for uniformity of tablet width. In addition to the rheological properties of the filaments, their mechanical properties also affected the RSD of tablet width, which could indicate discrepancies due to filament feeding issues, such as slipping. Filament loss modulus, loss factor, flexural stress, hardness, surface stiffness and printing temperature all correlated with the uniformity of tablet width (Fig. 4A) and constituted Model Equation 2.

$$width\ RSD^{0.5} = 0.4397 - 0.002152 \times Tp - 0.000001 \times G''(f = 82.5\ Hz) + 0.01313 \times \tan\delta\ (f = 0.121\ Hz) - 0.177 \times H + 0.001017 \times \sigma f\ (2.5\ \%\ deflection) + 0.001286 \times S \quad (2)$$

where T_p is printing temperature, G'' is loss modulus taken at f = 82.5 Hz (frequency sweep test), tan δ is loss factor taken at f = 0.121 Hz (frequency sweep test), H is filament hardness, σ_f is flexural stress taken at 2.5 % deflection and S is filament surface stiffness.

Higher printing temperature, filament loss modulus (as determined in frequency sweep test) and hardness reduce RSD of tablet width, while higher loss factor (as determined in frequency sweep test), flexural stress and surface stiffness of the filament all increase the RSD of tablet width.

3.3.2. Uniformity of drug release

Variability in layer formation, interfusion and interlayer porosity might cause a lack of uniformity in drug release. Medium could ingress much faster in certain parts of tablets, which are poorly bound. This impact might be even more noticeable between tablets from the same filament, where printed layers could be better merged for some printed tablets and poorly bound for others. This appears to be the case, as time to reach 60 % of drug release was hardly uniform for several formulations with RSD of drug release ranging from 4 to as much as 56 % (Table 4). Large deviations in drug release from tablets of the same batch can lead to inconsistent drug effects in patients, side effects, and safety issues. Formulations containing polymers Soluplus® and Shin-Etsu AQOAT® AS-LG exhibited especially poor uniformity of drug release. The reason could be attributed to the mechanism of drug release. Both polymers are poorly water soluble (supported

also by disintegration results) and release ketoprofen solely via diffusion. Water-insoluble polymers retain the tablet structure during dissolution studies, which acts as a barrier for dissolution medium entry and drug diffusion. Variability in the permeability of the barrier – polymer matrix is most likely determined by irregular porosity between neighbouring layers. As the tablet structure with presumably inconsistent porosity does not disintegrate during dissolution studies, variability in drug release is introduced. On the other hand, this impact is not as prevalent for filament formulations, which propel drug release via matrix dissolution or erosion mechanism. Tablet structure disintegrates during dissolution studies and the barrier for medium entry drug release is quickly removed. Therefore, the importance of interlayer porosity for uniformity of drug release is not as relevant in such formulations.

Several mechanical and rheological filament properties constitute the model of drug release RSD. Filament melt viscosity, loss factor (amplitude and frequency sweep test), elastic modulus and relative standard deviation of surface stiffness all correlated with the uniformity of drug release as presented in Fig. 4B and in a Model Equation 3.

$$release\ RSD = 0.2891 + 0.000142 \times \eta\ (\dot{\gamma}\ = 10\ s^{-1}) - 0.0470 \times \tan\delta\ (f = 56\ Hz) + 0.05733 \times \tan\delta\ (\gamma = 68.5\ \%) - 0.0614 \times Er - 0.587 \times SRSD \quad (3)$$

where η is melt viscosity taken at $\dot{\gamma}$ = 10 s^{-1}, tan δ is loss factor taken at f = 56 Hz and at γ = 68.5 % (frequency and amplitude sweep tests), E_r is filament elastic modulus and SRSD is relative standard deviation of filament surface stiffness.

By decreasing melt viscosity and loss factor from amplitude sweep test or increasing loss factor from frequency sweep test, filament elastic modulus and RSD of surface stiffness, the uniformity of drug release is improved. While rheological properties determine the integrity of layers and their merging capacity, the influence of mechanical properties on the uniformity of drug release is harder to explain. It could be, that inconsistent filament feeding results in the irregular porosity between subsequent layers or even causes the variability in layer height or thickness. Both scenarios can lead to poor uniformity of drug release.

3.3.3. Occurrence of tablet disintegration

Among 17 tablet samples, four formulations M3, M4, M5 and M6 did not disintegrate after 24 hours. Formulations M3 and M5 are mostly composed of polymer Soluplus® (polyvinyl caprolactam polyvinyl acetate-polyethylene glycol graft co-polymer), while M4 and M6 are mostly comprised of polymer Shin-Etsu AQOAT® AS-LG (hydroxypropyl methylcellulose acetate succinate). Both polymers exhibit a water insoluble behaviour. Therefore, it was explored on the filament level, whether the occurrence of disintegration can be extrapolated from the mechanical and rheological properties of filaments. It would be beneficial to create a predictive model, which would be able to distinguish between disintegrating and non-disintegrating formulations. A numeric value for disintegration was assigned to each filament, 1 in case of disintegrating and 0 in case of non-disintegrating character.

The model was constituted based on 3 input variables that correlated with the occurrence of tablet disintegration: melt viscosity, loss factor (temperature sweep test) and RSD of filament surface stiffness (Fig. 4C). Filaments with lower melt viscosity, loss factor and filament surface stiffness RSD are more likely to disintegrate. Disintegration index (DI) is described in Model Equation 4.

$$DI = 1.535 - 0.1286 \times \tan\delta\,(T = Tp) - 0.000323 \times \eta\left(\dot{\gamma} = 10\ s^{-1}\right) - 1.605 \times SRSD \quad (4)$$

where DI is disintegration index, tan δ is the loss factor taken at printing temperature (temperature sweep test), η is melt viscosity taken at $\dot{\gamma} = 10\ s^{-1}$ and SRSD is relative standard deviation of filament surface stiffness.

DI can be used to estimate the disintegrating or non-disintegrating character of tablets and establish a cut-off value. Values close to 1 indicate a disintegrating character of tablets and vice versa. DI was calculated and assigned to each filament. Calculated DI values matched the observed tablet disintegration properties (Fig. 5). Non-disintegrating tablets exhibited DI values lower or equal to 0.41, while disintegrating tablets provided values greater or equal to 0.72. The DI range between 0.41 and 0.72 should be further explored in future studies with more formulations to establish a more accurate cut-off value. So far, it can be concluded that tablets from filaments with DI greater or equal to 0.72 will disintegrate after 24 hours, while tablets from filaments with DI lower or equal to 0.41 will not.

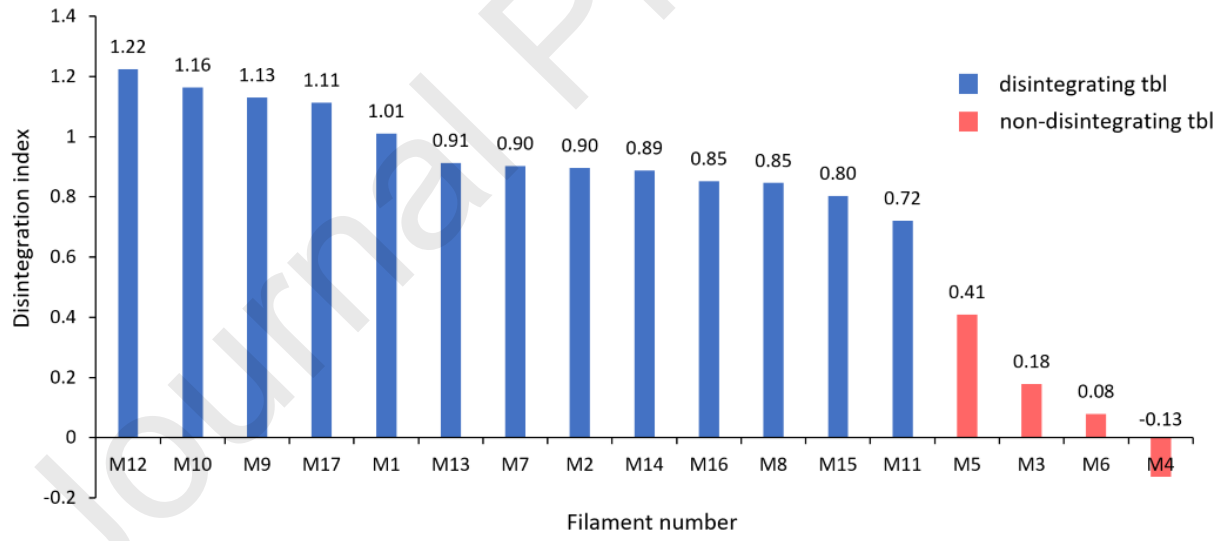

Fig. 5. Disintegration index calculated from model equation. Values towards 1 indicate a formulation dissolution or erosion character, while values close to 0 designate a non-soluble feature. Blue bars demonstrate tablet formulations that disintegrate, while red bars label formulations that do not disintegrate.

3.3.4. Uniformity of tablet disintegration time

Similarly to the uniformity of drug release, variability in tablet interlayer porosity may introduce a higher RSD of tablet disintegration time. This premise was tested on 13 disintegrating formulations on the filament level. Uniformity of tablet disintegration time ranged from 3 % to 29 % across formulations. Uniformity of drug release and tablet disintegration time did not match for several formulations. For example, formulation M2 had a low RSD of disintegration time at 3.01 % and high RSD of drug release at 22.08 %, while formulation M17 exhibited a high RSD of disintegration time at 16.32 % and low RSD of drug release at 7.30 %. This might point to a different mechanism causing the poor uniformity of both tablet attributes. Both relevant predictive models are also composed of completely different input variables. The statistical model of the RSD of the tablet disintegration time was established from filament melt loss modulus (frequency sweep test), filament surface stiffness and printing temperature (Fig. 4D). Uniformity of tablet disintegration time might be related to the variability in the intertwining of the polymeric chains, which constitute the tablet matrix system. The overlap of polymeric chains among other things determines how fast a polymer chain will dissolve or erode from the matrix. Therefore, the irregularities in polymer chain overlap might result in variable tablet disintegration time. Discrepancies in intertwining of the polymeric chains could be explained by the mechanical and rheological properties of filaments and the printing temperature. Filament surface stiffness could be responsible for the uniformity of material flow towards the liquefier. Filament melt loss modulus could determine the specifics of the polymer chains untying during melt formation and intertwining during material solidification in conjunction with the printing temperature. Based on predictive model (Equation 5), uniformity of disintegration time can be improved by decreasing the printing temperature and loss modulus (frequency sweep test) or increasing the filament surface stiffness.

$$DT\ RSD = -0.368 + 0.002943 \times Tp + 0.000003 \times G''(f = 82.5\ Hz) - 0.00197 \times S \qquad (5)$$

where T_p is printing temperature, G'' is loss modulus taken at f = 82.5 Hz (frequency sweep test) and S is filament surface stiffness.

4. Conclusion

Filament formulation can be a challenging process, as several filament formulations proved to be non-feedable due to their brittle or pliable character. Additionally, it was stipulated that filament processability does not necessarily ensure sufficient quality of 3D printed tablets. 23 filament formulations were prepared to study the influence of mechanical and rheological properties of filaments on filament processability and on eight tablet attributes. The filament formulation process followed the polymer mixing approach. Non-feedable pliable and brittle polymers were mixed in a feedable formulation, which cancelled out the disadvantages of each individual polymer. At least 20 % addition of a pliable polymer to a brittle formulation led to a printable filament and vice versa.

Predictive statistical models were established to avoid the trial-and-error filament formulation approach. Modelling of filament processability was primarily investigated. Filament surface

stiffness test was confirmed as the only predictive parameter, which designates the filament as feedable or non-feedable. Furthermore, it has been shown that the quadratic term of the filament surface stiffness is as important in the statistical model as the surface stiffness itself. Processability index (PI) was defined based on model equation as an indicator of filament printability with a cut-off value of 0.72. However, this value is equipment specific, as FDM 3D printers are composed of various feeding systems and some mechanisms exert stronger forces on filaments than others.

Uniformity of tablet properties was also studied as an indicator of the reproducibility of the printing process. Uniformity of tablet width, uniformity of drug release, uniformity of disintegration time and occurrence of disintegration all yielded statistical models with a great fit ($R^2 > 0.80$) and predictive value ($R^2_{(pred)} > 0.50$). As derived statistical models are independent of the choice of 3D printer, model equations represent a great utility and can be used for other research activities before printing trials. However, extensive mechanical and rheological testing of filaments is necessary. Filament surface stiffness test, three-point bend test, nanoindentation, melt viscosity, amplitude, temperature and frequency sweep tests all need to be performed to predict the uniformity of printed tablet attributes.

Statistical models with poor predictive value were obtained for uniformity of tablet mass, uniformity of tablet length, uniformity of tablet height, extent of drug release and tablet disintegration time due to a lack of correlation between measured filament and tablet properties. Further research is needed to investigate which key filament-, equipment- or process-characteristics are indicative of the tablet properties in question. Once these will be identified, the printed tablet qualities can be predicted on the filament and equipment level in conjunction with the models successfully established in this study.

Funding.

The authors thank Lek Pharmaceuticals d.d. for materials supplied for this study. This research was partly funded by the Slovenian Research Agency under grant number P1-0189. The APC was funded by the Faculty of Pharmacy, University of Ljubljana.

CRediT authorship contribution statement.

Klemen Kreft: Data curation, Formal analysis, Investigation, Visualization, Writing - original draft. **Zoran Lavrič:** Formal analysis, Investigation, Writing - review & editing. **Urška Gradišar Centa:** Data curation, Formal analysis, Investigation, Visualization, Writing - review & editing. **Mohor Mihelčič:** Data curation, Formal analysis, Investigation, Visualization, Writing - review & editing. **Lidija Slemenik Perše:** Conceptualization, Methodology, Supervision, Writing – review & editing. **Rok Dreu:** Conceptualization, Methodology, Supervision, Writing – review & editing.

Declaration of Competing Interest.

The authors declare that they have no known competing financial interests or personal relationships that could have appeared to influence the work reported in this paper.

Acknowledgments.

None.

Data availability.

The authors are unable or have chosen not to specify which data has been used.

References

Aho, J., Bøtker, J.P., Genina, N., Edinger, M., Arnfast, L., Rantanen, J., 2019. Roadmap to 3D-Printed Oral Pharmaceutical Dosage Forms: Feedstock Filament Properties and Characterization for Fused Deposition Modeling. J Pharm Sci. https://doi.org/10.1016/j.xphs.2018.11.012

Alhijjaj, M., Belton, P., Qi, S., 2016. An investigation into the use of polymer blends to improve the printability of and regulate drug release from pharmaceutical solid dispersions prepared via fused deposition modeling (FDM) 3D printing. European Journal of Pharmaceutics and Biopharmaceutics 108, 111–125. https://doi.org/10.1016/j.ejpb.2016.08.016

Azad, M.A., Olawuni, D., Kimbell, G., Badruddoza, A.Z.M., Hossain, M.S., Sultana, T., 2020. Polymers for extrusion-based 3D printing of pharmaceuticals: A holistic materials–process perspective. Pharmaceutics. https://doi.org/10.3390/pharmaceutics12020124

Crișan, A.G., Porfire, A., Ambrus, R., Katona, G., Rus, L.M., Porav, A.S., Ilyés, K., Tomuță, I., 2021. Polyvinyl alcohol-based 3d printed tablets: Novel insight into the influence of polymer particle size on filament preparation and drug release performance. Pharmaceuticals 14. https://doi.org/10.3390/ph14050418

Fuenmayor, E., Forde, M., Healy, A. v., Devine, D.M., Lyons, J.G., McConville, C., Major, I., 2018. Material considerations for fused-filament fabrication of solid dosage forms. Pharmaceutics 10. https://doi.org/10.3390/pharmaceutics10020044

Go, J., Schiffres, S.N., Stevens, A.G., Hart, A.J., 2017. Rate limits of additive manufacturing by fused filament fabrication and guidelines for high-throughput system design. Addit Manuf 16, 1–11. https://doi.org/10.1016/j.addma.2017.03.007

Goyanes, A., Fina, F., Martorana, A., Sedough, D., Gaisford, S., Basit, A.W., 2017. Development of modified release 3D printed tablets (printlets) with pharmaceutical excipients using additive manufacturing. Int J Pharm 527, 21–30. https://doi.org/10.1016/j.ijpharm.2017.05.021

Gültekin, H.E., Tort, S., Acartürk, F., 2019. An Effective Technology for the Development of Immediate Release Solid Dosage Forms Containing Low-Dose Drug: Fused Deposition Modeling 3D Printing. Pharm Res 36. https://doi.org/10.1007/s11095-019-2655-y

Henry, S., Samaro, A., Marchesini, F.H., Shaqour, B., Macedo, J., Vanhoorne, V., Vervaet, C., 2021. Extrusion-based 3D printing of oral solid dosage forms: Material requirements and equipment dependencies. Int J Pharm 598. https://doi.org/10.1016/j.ijpharm.2021.120361

Ilyés, K., Kovács, N.K., Balogh, A., Borbás, E., Farkas, B., Casian, T., Marosi, G., Tomuță, I., Nagy, Z.K., 2019. The applicability of pharmaceutical polymeric blends for the fused deposition modelling (FDM) 3D technique: Material considerations–printability–process modulation, with consecutive effects on in vitro release, stability and degradation. European Journal of Pharmaceutical Sciences 129, 110–123. https://doi.org/10.1016/j.ejps.2018.12.019

Isreb, A., Baj, K., Wojsz, M., Isreb, M., Peak, M., Alhnan, M.A., 2019. 3D printed oral theophylline doses with innovative 'radiator-like' design: Impact of polyethylene oxide (PEO) molecular weight. Int J Pharm 564, 98–105. https://doi.org/10.1016/j.ijpharm.2019.04.017

Jamróz, W., Szafraniec, J., Kurek, M., Jachowicz, R., 2018. 3D Printing in Pharmaceutical and Medical Applications – Recent Achievements and Challenges. Pharm Res. https://doi.org/10.1007/s11095-018-2454-x

Kempin, W., Domsta, V., Grathoff, G., Brecht, I., Semmling, B., Tillmann, S., Weitschies, W., Seidlitz, A., 2018. Immediate Release 3D-Printed Tablets Produced Via Fused Deposition Modeling of a Thermo-Sensitive Drug. Pharm Res 35. https://doi.org/10.1007/s11095-018-2405-6

Lamichhane, S., Bashyal, S., Keum, T., Noh, G., Seo, J.E., Bastola, R., Choi, J., Sohn, D.H., Lee, S., 2019. Complex formulations, simple techniques: Can 3D printing technology be the Midas touch in pharmaceutical industry? Asian J Pharm Sci. https://doi.org/10.1016/j.ajps.2018.11.008

Melocchi, A., Parietti, F., Maroni, A., Foppoli, A., Gazzaniga, A., Zema, L., 2016. Hot-melt extruded filaments based on pharmaceutical grade polymers for 3D printing by fused deposition modeling. Int J Pharm 509, 255–263. https://doi.org/10.1016/j.ijpharm.2016.05.036

Muñiz Castro, B., Elbadawi, M., Ong, J.J., Pollard, T., Song, Z., Gaisford, S., Pérez, G., Basit, A.W., Cabalar, P., Goyanes, A., 2021. Machine learning predicts 3D printing performance of over 900 drug delivery systems. Journal of Controlled Release 337, 530–545. https://doi.org/10.1016/J.JCONREL.2021.07.046

Nasereddin, J.M., Wellner, N., Alhijjaj, M., Belton, P., Qi, S., 2018. Development of a Simple Mechanical Screening Method for Predicting the Feedability of a Pharmaceutical FDM 3D Printing Filament. Pharm Res 35. https://doi.org/10.1007/s11095-018-2432-3

Ong, J.J., Castro, B.M., Gaisford, S., Cabalar, P., Basit, A.W., Pérez, G., Goyanes, A., 2022. Accelerating 3D printing of pharmaceutical products using machine learning. Int J Pharm X 4, 100120. https://doi.org/10.1016/J.IJPX.2022.100120

Palekar, S., Nukala, P.K., Mishra, S.M., Kipping, T., Patel, K., 2019. Application of 3D printing technology and quality by design approach for development of age-appropriate pediatric formulation of baclofen. Int J Pharm 556, 106–116. https://doi.org/10.1016/j.ijpharm.2018.11.062

Parulski, C., Jennotte, O., Lechanteur, A., Evrard, B., 2021. Challenges of fused deposition modeling 3D printing in pharmaceutical applications: Where are we now? Adv Drug Deliv Rev. https://doi.org/10.1016/j.addr.2021.05.020

Pietrzak, K., Isreb, A., Alhnan, M.A., 2015. A flexible-dose dispenser for immediate and extended release 3D printed tablets. European Journal of Pharmaceutics and Biopharmaceutics 96, 380–387. https://doi.org/10.1016/j.ejpb.2015.07.027

Prasad, E., Islam, M.T., Goodwin, D.J., Megarry, A.J., Halbert, G.W., Florence, A.J., Robertson, J., 2019. Development of a hot-melt extrusion (HME) process to produce drug loaded Affinisol™ 15LV filaments for fused filament fabrication (FFF) 3D printing. Addit Manuf 29. https://doi.org/10.1016/j.addma.2019.06.027

Samaro, A., Janssens, P., Vanhoorne, V., van Renterghem, J., Eeckhout, M., Cardon, L., de Beer, T., Vervaet, C., 2020. Screening of pharmaceutical polymers for extrusion-Based Additive Manufacturing of patient-tailored tablets. Int J Pharm 586. https://doi.org/10.1016/j.ijpharm.2020.119591

Shi, K., Slavage, J.P., Maniruzzaman, M., Nokhodchi, A., 2021. Role of release modifiers to modulate drug release from fused deposition modelling (FDM) 3D printed tablets. Int J Pharm 597. https://doi.org/10.1016/j.ijpharm.2021.120315

Siamidi, A., Tsintavi, E., M. Rekkas, D., Vlachou, M., 2020. 3D-Printed Modified-Release Tablets: A Review of the Recent Advances, in: Molecular Pharmacology. IntechOpen. https://doi.org/10.5772/intechopen.90868

Solanki, N.G., Tahsin, M., Shah, A. v., Serajuddin, A.T.M., 2018. Formulation of 3D Printed Tablet for Rapid Drug Release by Fused Deposition Modeling: Screening Polymers for Drug Release, Drug-Polymer Miscibility and Printability. J Pharm Sci 107, 390–401. https://doi.org/10.1016/j.xphs.2017.10.021

Tan, D.K., Maniruzzaman, M., Nokhodchi, A., 2018. Advanced pharmaceutical applications of hot-melt extrusion coupled with fused deposition modelling (FDM) 3D printing for personalised drug delivery. Pharmaceutics. https://doi.org/10.3390/pharmaceutics10040203

Than, Y.M., Titapiwatanakun, V., 2021. Tailoring immediate release FDM 3D printed tablets using a quality by design (QbD) approach. Int J Pharm 599. https://doi.org/10.1016/j.ijpharm.2021.120402

Trenfield, S.J., Awad, A., Goyanes, A., Gaisford, S., Basit, A.W., 2018. 3D Printing Pharmaceuticals: Drug Development to Frontline Care. Trends Pharmacol Sci. https://doi.org/10.1016/j.tips.2018.02.006

Venkataraman, N., Rangarajan, S., Matthewson, M.J., Harper, B., Safari, A., Danforth, S.C., Wu, G., Langrana, N., Guceri, S., Yardimci, A., n.d. Feedstock material property ± process relationships in fused deposition of ceramics (FDC).

Xu, P., Li, J., Meda, A., Osei-Yeboah, F., Peterson, M.L., Repka, M., Zhan, X., 2020. Development of a quantitative method to evaluate the printability of filaments for fused deposition modeling 3D printing. Int J Pharm 588. https://doi.org/10.1016/j.ijpharm.2020.119760

Zhang, J., Feng, X., Patil, H., Tiwari, R. v., Repka, M.A., 2017. Coupling 3D printing with hot-melt extrusion to produce controlled-release tablets. Int J Pharm 519, 186–197. https://doi.org/10.1016/j.ijpharm.2016.12.049

Zhang, J., Xu, P., Vo, A.Q., Bandari, S., Yang, F., Durig, T., Repka, M.A., 2019. Development and evaluation of pharmaceutical 3D printability for hot melt extruded cellulose-based filaments. J Drug Deliv Sci Technol 52, 292–302. https://doi.org/10.1016/j.jddst.2019.04.043

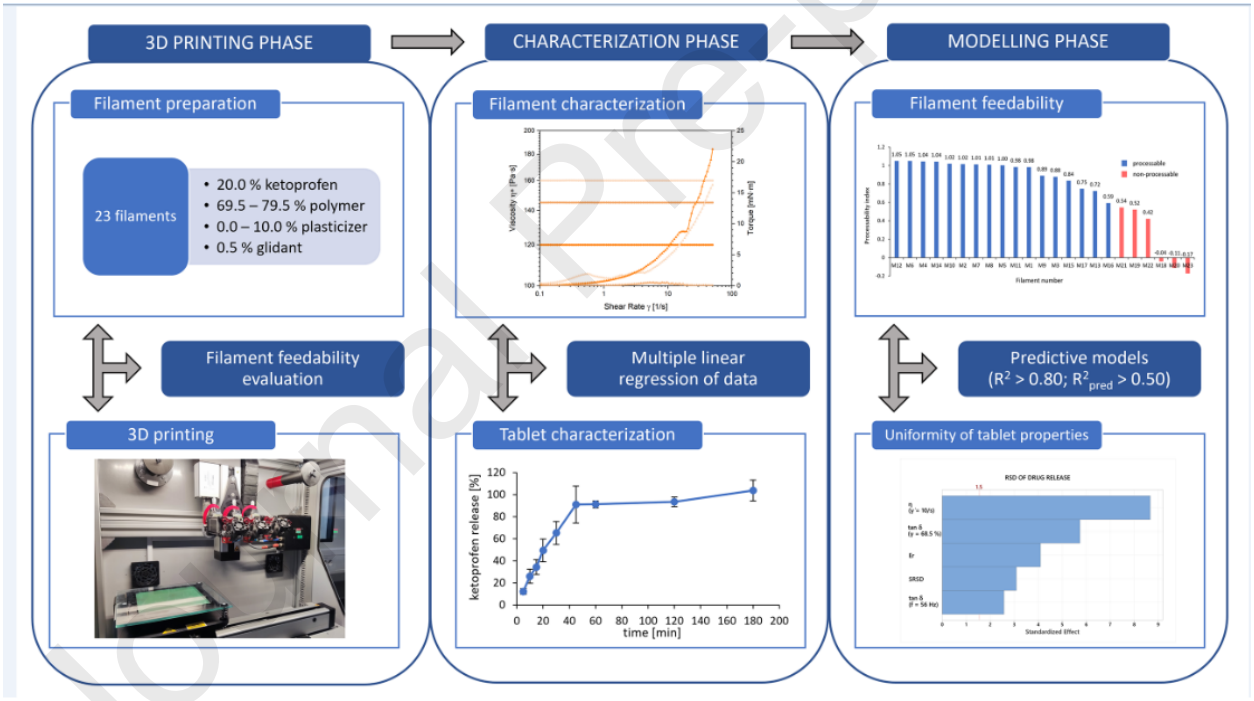

CRediT authorship contribution statement.

Klemen Kreft: Data curation, Formal analysis, Investigation, Visualization, Writing - original draft. **Zoran Lavrič:** Formal analysis, Investigation, Writing - review & editing. **Urška Gradišar**

Centa: Data curation, Formal analysis, Investigation, Visualization, Writing - review & editing. **Mohor Mihelčič:** Data curation, Formal analysis, Investigation, Visualization, Writing - review & editing. **Lidija Slemenik Perše:** Conceptualization, Methodology, Supervision, Writing – review & editing. **Rok Dreu:** Conceptualization, Methodology, Supervision, Writing – review & editing.

Declaration of interests

☐ The authors declare that they have no known competing financial interests or personal relationships that could have appeared to influence the work reported in this paper.

☒ The authors declare the following financial interests/personal relationships which may be considered as potential competing interests:

Klemen Kreft reports equipment, drugs, or supplies was provided by Lek Pharmaceuticals d.d. Rok Dreu reports financial support was provided by Public Research Agency of the Republic of Slovenia.